

Rotational spectroscopy of gas-phase molecules is a time-honored technique which has been fundamental for developing our knowledge of molecular structure [7]. Its range continues to be extended, both in laboratory, in astronomical observatories and in space instruments, for example to cold molecules [8]. Nevertheless, rotational spectroscopy has, in the vast majority of cases, not been able to achieve ultra-high spectroscopic resolution and accuracy. Enabling this would open up numerous opportunities for studies in molecular physics and in fundamental physics, such as tests of molecular quantum theory, measurement of magnetic and optical susceptibilities, investigation of collision interactions, tests of the time-independence of particle masses [9–13], and the measurement of fundamental constants [5, 14–16].

In conventional (linear) rotational spectroscopy resolution can be improved by cooling of the molecules to a cryogenic translational temperature T , but the gains possible with thermal cooling methods ($T \gtrsim 10$ K) are modest [8], due to the \sqrt{T} - dependence of the Doppler line width. For untrapped, neutral molecules, a leap in resolution and accuracy in rotational spectroscopy was achieved with the introduction of Lamb-dip (saturation) spectroscopy [17, 18]. It allowed improving the fractional line resolution by approximately a factor 20 - 30 beyond the Doppler broadening, to 5×10^{-8} [17]. This level has, however, not improved for nearly 50 years [19, 20], since it is limited by time-of-flight broadening. In the context of molecular ions, ion trapping combined with sympathetic cooling by Doppler-laser-cooled atomic ions to the “crystallized” cluster state provides a well-tested approach for further reducing T to the 10 mK level, with concomitant reduction of Doppler line width by approximately a factor 30 [5].

Here, for the first time, we not only realize this improvement for rotational spectroscopy but also achieve Doppler-free spectral resolution, by reaching the rotational Lamb-Dicke regime (LDR). The LDR is defined by $\delta x < \lambda_{\text{rot}}/2\pi$, where δx is the range of the ions’ motion along the spectroscopy beam direction $\hat{\mathbf{k}} \parallel x$ [21]. In this work, the motion ranges are thermal in origin. In prolate ion clusters of appropriate size, the ranges of motion orthogonal to the clusters’ long axes (z) are $\delta x, \delta y < 20 \mu\text{m}$. Directing $\hat{\mathbf{k}}$ orthogonal to z satisfies the LDR condition for rotational transition wavelengths, with typical values $\lambda_{\text{rot}} \simeq 0.2 - 2 \text{ mm}$. Ultra-high fractional and absolute frequency resolution are thereby enabled. In contrast, vibrational spectroscopy, where wavelengths are $\lambda_{\text{vib}} < 8 \mu\text{m}$, yields lines exhibiting the classic Doppler width [5, 22], often further complicated by unresolved hyperfine structure [15, 16].

The present methods does not require complex techniques such as single-ion manipulation, ground-state cooling, and quantum spectroscopy [23, 24] to capitalize on the advantage of the LDR regime. The performance improvement in terms of fractional resolution is a factor 50 compared to both previous trapped molecular ion ensemble spectroscopy [5, 22] and to the highest resolution rotational spectroscopy of neutral molecules reported so far [20], to the best of our knowledge.

In order to perform a stringent test of the new method, we choose the polar molecule with the smallest fundamental rotational transition wavelength $\lambda_{\text{rot,min}} \simeq 228 \mu\text{m}$ ($f_{\text{rot,max}} \simeq 1.3 \text{ THz}$): HD^+ . In addition, the feasibility of *ab initio* calculation of f_{rot} for HD^+ and of its sensitivities to external fields allows testing the spectroscopic *accuracy* of the method.

The basic concept is depicted in Fig. 1. In a prolate ion cluster of appropriate size, trapped in a linear quadrupole trap (trap axis is along z), the sympathetically cooled ions arrange approximately as a narrow cylinder aligned along the trap axis. Maximum ion radial distances from the axis are significantly smaller than the cylinder length. Molecular dynamics simulations for a cluster containing $N = 200 \text{ HD}^+$ ions (Cluster 1, see Methods) indicate r.m.s. position variations (corresponding approximately to the range $\delta x/2$) $\Delta x = \Delta y \simeq 8.4 \mu\text{m}$ at $T = 12 \text{ mK}$, increasing slightly to $9.0 \mu\text{m}$ at 67 mK . These values are significantly smaller than $\lambda_{\text{rot}}/2\pi \simeq 36 \mu\text{m}$, indicating the LDR if $\hat{\mathbf{k}}$ is chosen perpendicular to the trap axis.

In the LDR, the absence of Doppler broadening and, because of ion confinement, also of transit-time broadening, puts into evidence other broadening mechanisms. Among these, pressure (collision) broadening, can be suppressed by operating under a sufficiently small residual background neutral gas pressure. Collisions between the trapped ions themselves do not lead to appreciable frequency shifts, because minimum approach distances are of order $10 \mu\text{m}$.

A major broadening effect can then be power (saturation) broadening by the spectroscopy wave. The corresponding line width is $\Delta\nu_{\text{pb}} = \sqrt{2}\Omega_{\text{R}}/2\pi$, with the Rabi angular frequency $\Omega_{\text{R}} = \mu_{\text{eg}}E/\hbar$, the transition dipole moment μ_{eg} , and the electric field amplitude E . A beam power $P = \frac{1}{2}\epsilon_0 c E^2 A = 1 \text{ pW}$, and a beam cross sectional area $A = \pi \times 1 \text{ mm}^2$ (limited from above by the distance between the trap electrodes, and by diffraction), yield $\Delta\nu_{\text{pb}} = 43 \text{ Hz}$, assuming $\mu_{\text{eg}} = 0.15 e a_0$ (as for a “strong” spin component of the HD^+ fundamental rotational transition). Thus, extremely low, pW-level power must be used on

“strong” transitions if the line broadening is to be reduced below the 10^{-10} level, even for f_{rot} as high as 10^{12} Hz. It is advantageous that such low power levels strongly simplify the technological requirements on the source.

Ultra-narrow transitions may be challenging to find. Theoretical predictions and results from e.g. lower resolution rovibrational spectroscopy may be helpful or necessary to reduce the spectral range of the search. Also, performing the spectroscopy initially at high intensity leads to broad spectral lines, which are easier to find. Subsequently, the intensity is progressively reduced to increase spectral resolution and accuracy.

In order to access experimentally the smallest possible line widths, it is necessary to lift as far as possible the Zeeman degeneracy of transitions by applying a magnetic field. Excitation of an individual Zeeman component implies excitation of the molecules populating a single quantum state. Techniques for increasing the population in this state and thus the signal may therefore be required. Here, we use rotational laser cooling (see Methods).

The potential of rotational spectroscopy in the LDR can only be harnessed fully if the microwave source has excellent spectral purity (small line width) and high absolute frequency stability. For this work, we have implemented a “frequency chain”, where $f_{\text{rot}} \simeq 1.3$ THz is referenced to a hydrogen maser (see Methods).

We address one particular spin component of the rotational transition, $|g\rangle = (v = 0, N = 0, J = 2) \xrightarrow{1.3 \text{ THz}} |e\rangle = (v' = 0, N' = 1, J' = 3)$, see Fig. 2. v, N, J denote vibrational, rotational and total angular momentum quantum number, respectively. Spectroscopy is performed by $1 + 1' + 1''$ resonance-enhanced multi-photon dissociation (REMPD), where the upper spectroscopy level undergoes $|e\rangle \xrightarrow{1.42 \mu\text{m}} (v'' = 4, N'' = 0, J''' = 2) \xrightarrow{266 \text{ nm}} \text{H} + \text{D}^+$. The reduction of the number of trapped HD^+ upon dissociation is measured using secular excitation, and represents the spectroscopy signal. Repeated HD^+ trap loading and spectroscopy cycles are performed and the signals averaged so as to increase the signal-to-noise ratio. Typical ion clusters used for spectroscopy are similar to the one shown in Fig. 1, having $T \simeq 10$ mK.

Fig. 3 shows the measured spectrum $|g\rangle \rightarrow |e\rangle$ in the neighborhood of the theoretically predicted frequency (see Methods)

$$f_{\text{rot,theory}} = 1\,314\,935.827\,3(10) \text{ MHz} . \quad (1)$$

At comparatively high intensity (approximately $0.1 \mu\text{W}/\text{mm}^2$, green points) the line width

is 12 kHz, whereas the calculated Doppler line width is 54 kHz. By reducing the source power successively the line width decreases to 1.3 kHz (blue points). This clearly evidences power broadening. The latter line width is mostly due to residual power broadening. In order to obtain sufficient signal strength, we did not lift the Zeeman degeneracy completely and the spectrum contains the unresolved superposition of the Zeeman transition pairs T_+ : $J_z = 2 \rightarrow J'_z = 3$ and T_- : $J_z = -2 \rightarrow J'_z = -3$ (J_z is the projection of the total angular momentum on the quantization axis). . The closest other Zeeman component has a detuning of -13 kHz or more.

The shift of the transitions T_{\pm} with magnetic field B has been theoretically calculated to be strictly linear in B , $\Delta f(T_{\pm}, B) = \pm E_{10}(v = 0, N = 1) B = \mp 0.56 \text{ kHz } (B/1 \text{ G})$ ([25] and Methods). The mean frequency is therefore free of any Zeeman shift. The magnetic field is $B = 0.40(6) \text{ G}$, measured with an anisotropic magnetoresistive probe and by radio-frequency spectroscopy of the Be^+ ions using the method of ref. [26].

We obtain the rotational frequency

$$f_{\text{rot,exp}} = 1\,314\,935.828\,0(6) \text{ MHz} . \quad (2)$$

The uncertainty (4×10^{-10}) results from the experimental resolution and from the Zeeman pair asymmetry uncertainty (2.5×10^{-10}). Other perturbations of the transition frequency are compatible with zero within an estimated uncertainty 3×10^{-11} (see Methods).

The value $f_{\text{rot,exp}}$ is in agreement with the *ab initio* prediction $f_{\text{rot,theory}}$ within the combined error, 1.1 kHz. We thus confirm the accuracy of the molecular calculations, including its QED contributions, at the level of 1.1 kHz (9×10^{-10}), limited by theory. This represents the most precise test of a molecular physics prediction yet.

The *ab initio* value $f_{\text{rot,theory}}$ is based on the CODATA2014 values of the fundamental constants [27], in particular on the proton mass m_p . Among the stable fundamental particles of atomic physics, this is the particle that currently has the largest fractional uncertainty (0.09 ppb). We can obtain a value for m_p from the present experiment by treating it as a fit parameter, while taking the other constants, m_d , m_e , R_{∞} , α , and their uncertainties from CODATA2014. The spectroscopically determined value then is

$$m_p = 1.007\,276\,466\,9(13) \text{ u} , \quad (3)$$

with fractional uncertainty 1.3×10^{-9} . This is the most accurate spectroscopic result for m_p to date, and improves by a factor 3.3 on the recent result [16].

In conclusion, with the newly introduced method, we increase the resolution of rotational spectroscopy by a factor of 50. Our experiment - theory agreement between $f_{\text{rot,exp}}$ and $f_{\text{rot,theory}}$ is a direct proof that the present method permits rotational frequency inaccuracy at least at the 9×10^{-10} level, without the necessity for corrections. The reason for this are the method's resolution and the favorable conditions in the UHV ion trap and not that the HD^+ test molecule is particularly *insensitive* to perturbations. Therefore, similar inaccuracy levels should be achievable for other molecular species.

The present work opens outstanding perspectives for precision physics. With improvements in signal strength, we expect that the spectroscopic resolution can be increased by at least one order, leading in addition to a systematic uncertainty $< 3 \times 10^{-11}$ (see Methods). This will allow testing the *ab initio* prediction of the rotational frequency of the HD^+ molecular ion with even higher precision. The major contribution to $f_{\text{rot,theory}}$, the spin-averaged contribution, has already been evaluated in this work with 1.4×10^{-11} uncertainty and further progress on the minor contributions, the hyperfine Hamiltonian coefficients, is expected [28–31]. Such an improved test will also provide a fairly direct test of theoretical approaches used to compute the frequencies of the related molecular ions H_2^+ and D_2^+ and of antiprotonic helium. Eventually, the fundamental constants R_∞ , m_e , m_p , m_d will become measurable at the 10^{-11} level by *molecular* spectroscopy, which is a complementary approach to the current ones, thus strengthening the overall consistency of this set of fundamental constants.

Thanks to the spectral resolution possible with the present method, it will become possible to measure molecular properties which are of small magnitude and thus are otherwise difficult access, e.g. level-dependent magnetic moments and a.c. polarisabilities (light shifts).

Our method also opens up vast possibilities in terms of accessible molecular species. Given the mass (m_c) of singly-ionized laser-coolable atomic ions, molecular ions with mass-to-charge ratio $m/q^2 < m_c/e^2$ can be confined inside the atomic ion cluster, in the rotational Lamb-Dicke regime. Employing, e.g., the high-mass ytterbium ion $^{171}\text{Yb}^+$ as coolant, many thousands of singly-ionized ($q = e$) molecular species, not counting isotopologues, have suitable mass. Many of these species exhibit a simpler spin structure than the test case used here, which can be advantageous in simplifying the spectrum and increasing state populations.

We note that radiation sources of appropriate spectral purity and stability can be implemented not only using an H-maser as reference but also more simply and accessibly using a GPS-steered high-performance quartz oscillator. For most molecules, the fundamental rotational transition frequency is smaller than 1 THz, which simplifies the source further. In a complementary direction, the method could also be applied to other rotational transitions $N > 0 \rightarrow N' = N + 1$, with correspondingly higher frequencies and thus potentially higher fractional spectral resolution. Possibly, also two-photon [32] and electric quadrupole rotational transitions could become accessible.

Finally, this method should be applicable also to rotational stimulated Raman transitions driven by co-propagating waves and to two-photon vibrational transitions. The latter would be driven by counter-propagating waves f_1, f_2 having a sufficiently small frequency difference $|f_1 - f_2| < c/2\pi\delta x$, ensuring the LDR. It is particularly advantageous that in diatomics transitions exist for which f_1 and f_2 can be chosen to satisfy this condition but also to be near-resonant with a dipole-allowed transition to an intermediate rovibrational level, so that the two-photon transition rate is enhanced.

I. METHODS

A. Simulation of ion dynamics in Coulomb clusters

The spatial distribution of ions in a two-species Coulomb crystal is well-known [34]. Given an elongated trap and electrode geometry, and for typical magnitudes of the RF voltages and of the end-cap voltages, a strongly prolate atomic ion cluster can result. Sympathetically cooled molecular ions, if lighter than the atomic coolant ions, and if in smaller number, are distributed in a string-like or cylinder-like volume, centered on the trap axis (z). (Equal charge states are assumed.) The boundary shapes of the two species' spatial distributions are constant in time.

Molecular dynamics (MD) simulations help to elucidate details, in particular effects of temperature and dynamics. We simulated two ion clusters. Cluster C1 contains $N_{\text{Be}^+} = 2000$ Be^+ ions which sympathetically cool $N = 200$ HD^+ ions, resulting in a tubular configuration for the latter. C1 is similar to the experimentally produced clusters (Fig. 1). A smaller cluster (C2) was modeled for comparison: with $N = 50$, $N_{\text{Be}^+} = 500$ the molecular

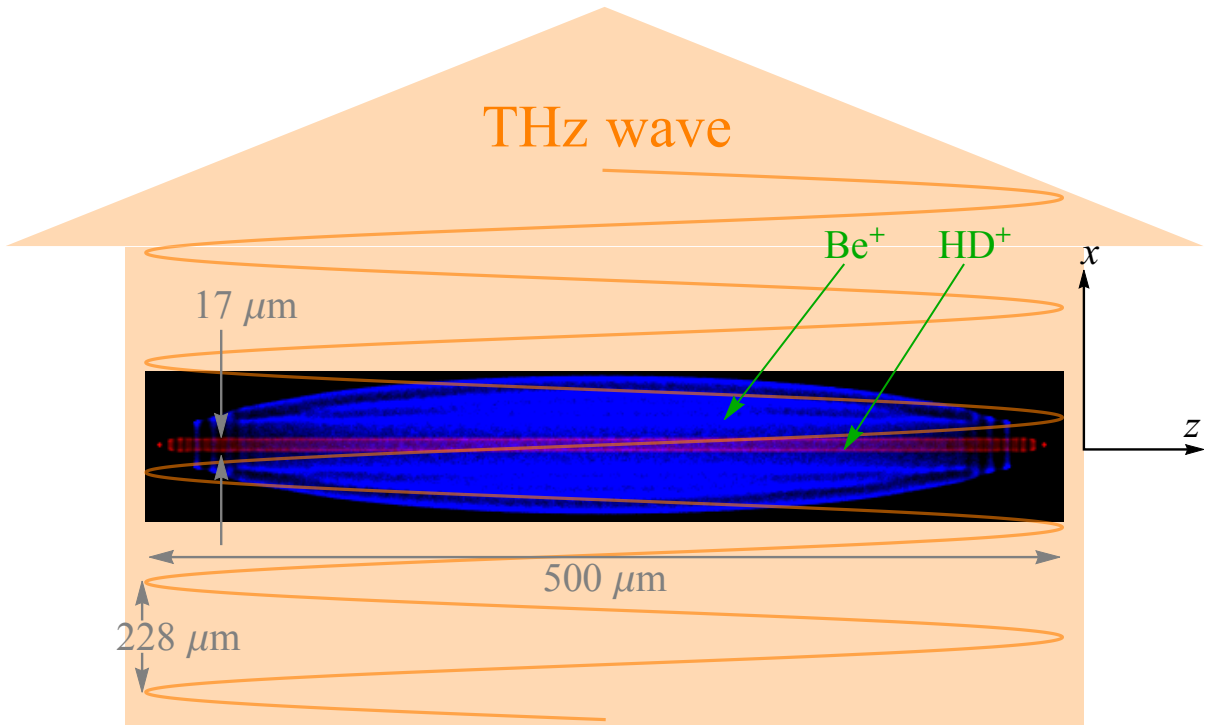


FIG. 1. Principle of the Lamb-Dicke rotational spectroscopy of sympathetically cooled molecular ions. The ion cluster is prolate, and the sympathetically cooled ions exhibit a relatively small motional range in the directions x, y perpendicular to the trap axis z . The spectroscopy radiation propagates perpendicular to z . The ion cluster image is a time average of ion trajectories obtained from an MD simulation of an ensemble of $N = 200$ HD^+ ions and $N_{\text{Be}^+} = 2000$ atomic ions (see Methods). Ion clusters generated in the experiment are similar to the one shown here.

ions arrange as a string. The simulations are performed in the pseudopotential approximation, since the micromotion of HD^+ ions only gives small corrections (here, the q -parameter is 0.15). The simulations extended over 5 ms. The equilibrium secular temperature T of the molecular ions is determined by the assumed cooling and heating rate parameters, which are varied in order to exhibit the temperature dependence of the clusters' properties [35]. A key feature of large clusters such as C1 is that even at the lowest temperatures achievable experimentally by sympathetic cooling, $T \simeq 10 - 30$ mK, the ions' positions are not completely “frozen”. Instead, the ions diffuse through the cluster volume, with the diffusion speed being a function of temperature [35].

The ion motion characteristics can be analyzed in detail. One characteristic is the co-

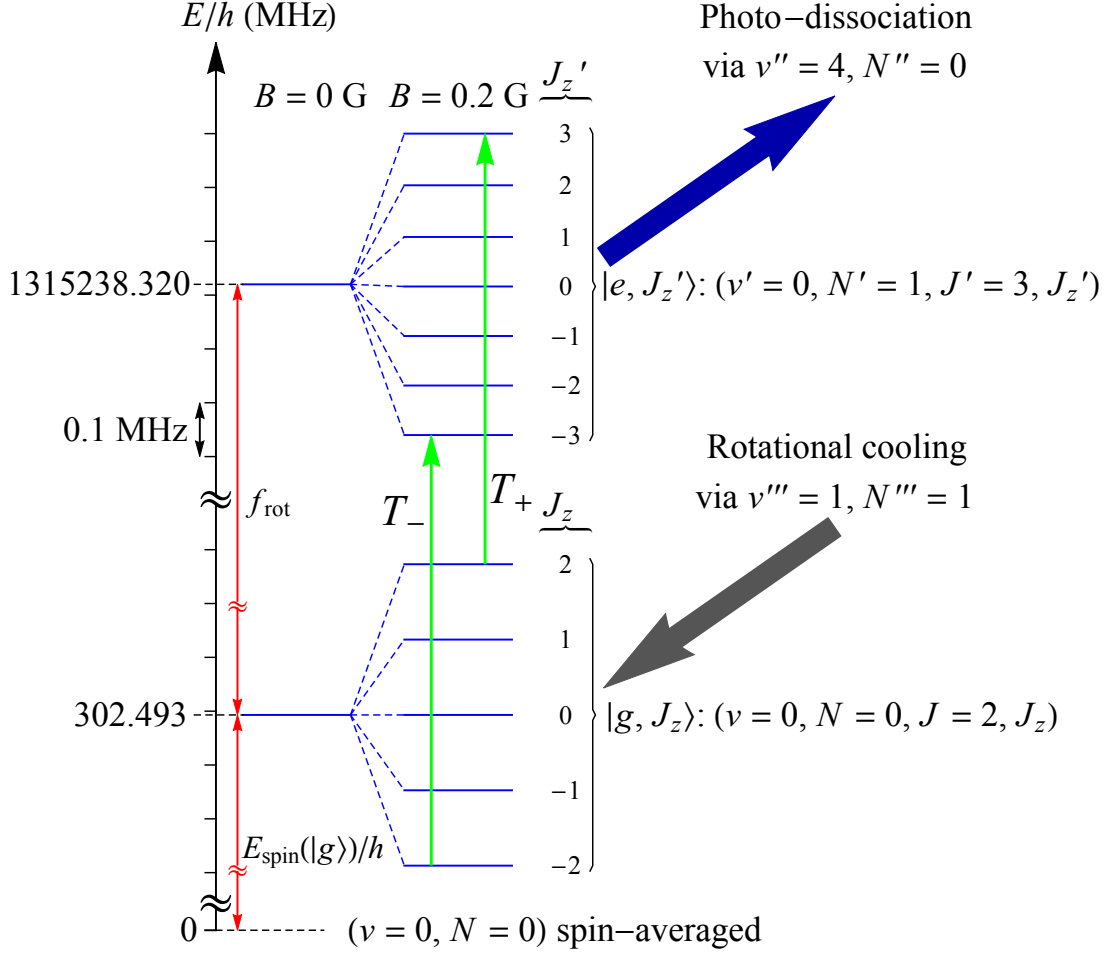


FIG. 2. Simplified diagram of relevant energy levels of HD^+ in the ground vibrational level $v = 0$. We show only one spin state, $J = 2$, of the ground rotational level $N = 0$, denoted by $|g\rangle$, and one spin state, $J' = 3$, of the first excited rotational level $N' = 1$, denoted by $|e\rangle$. The green arrows show the transitions addressed in this work, exhibiting a linear Zeeman splitting. The population of the $N = 0$ - spin states is enhanced by rotational cooling (thick gray arrow), and the population in the $N' = 1$ - states is photo-dissociated by two lasers (blue arrow). The zero of the energy scale corresponds to the energy of the $N = 0$ - level in absence of the effective spin Hamiltonian interaction of ref. [33].

ordinate r.m.s. variation, defined as $\Delta\xi = \langle \Delta\xi_i \rangle$, $\Delta\xi_i = \overline{\xi_i(t)^2} - \overline{\xi_i(t)}^2$, where i numbers the ion, $\xi = x, y, z$, the over-bar denotes the time average and $\langle \dots \rangle = N^{-1} \sum_{i=1}^N \dots$ denotes the ensemble average. The values for C1 put in evidence transverse confinement and diffusion features: whereas for motion along the trap axis $\Delta z_{\text{C1}} = (41, 142, 206) \mu\text{m}$ over

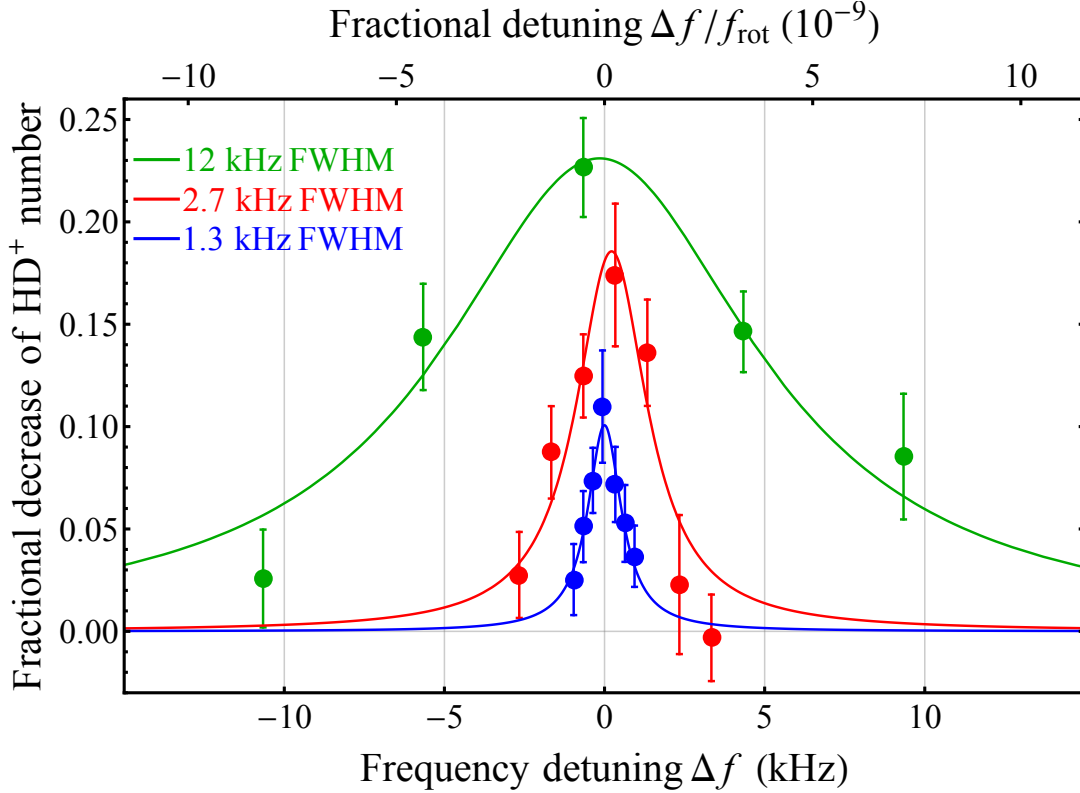


FIG. 3. Spectroscopy of one hyperfine component of the fundamental rotational transition of HD^+ . Shown is the unresolved transition pair T_{\pm} between the stretched states, $(J = 2, J_z = \pm J) \rightarrow (J' = 3, J'_z = \pm J')$, at different power levels of the THz wave. The magnetic field is $B \simeq 0.4$ G. The lines are Lorentzian fits. Zero detuning corresponds to the center frequency of the blue fit.

a time interval of 5 ms, at $T = (12, 33, 67)$ mK, respectively, the transverse excursions are $\Delta x_{\text{C1}} = \Delta y_{\text{C1}} = (8.4, 8.6, 9.0)$ μm . These latter values are significantly smaller than $\lambda_{\text{rot,min}}/2\pi$. In Fig. 4 (a, b) we show some details of HD^+ ion motion, the spectral density of the x coordinate and the time-averaged spatial distribution.

We can obtain an estimate for the spectroscopy line shape L induced by the ions' motion, neglecting recoil and spontaneous emission effects, by evaluating the ensemble-averaged Fourier spectrum of the spectroscopy wave's electric field amplitude seen by a moving ion, $E(\mathbf{r}_i, t) \propto \text{Re}[\exp(i\Phi(\mathbf{r}_i(t)) - i\omega t)]$, where $\Phi(\mathbf{r}_i) = \mathbf{k} \cdot \mathbf{r}_i$. For transverse excitation along x , $\Phi(\mathbf{r}_i) = 2\pi x_i/\lambda$. ω and λ are the angular frequency and wavelength of the wave. We define the line shape as $L(\Delta f) = \langle |\mathcal{F}_{\Delta f} \{\exp(i2\pi x_i(t)/\lambda)\}|^2 \rangle$, where the argument Δf of the Fourier transform corresponds to the spectroscopic detuning from resonance. For wave-

lengths $\lambda \lesssim 10 \mu\text{m}$ the line shape is close to Gaussian, with the width Δf_{FWHM} determined by the classic expression proportional to \sqrt{T} , see the dashed lines in Fig. 4 (c). For wavelengths $\lambda \geq 50 \mu\text{m}$ a substantial delta function peak $L(0)$ (Lamb-Dicke peak) develops at $\Delta f = 0$. It is given by $L(0) = \left\langle \left| \overline{\exp(i 2\pi x_i(t)/\lambda)} \right|^2 \right\rangle$ and is shown in Fig. 4 (d) (points) as a function of wavelength for the two clusters.

If the ions' coordinates $x_i(t)$ were Gaussian random variables, $L(0)$ would simplify to $L_g(0) = \langle \exp(-(2\pi\Delta x_i/\lambda)^2) \rangle$ [36]. Since in clusters of the sizes as in C1, C2, most ions behave similarly, $L_g(0) \simeq \exp(-(2\pi\Delta x/\lambda)^2)$. This expression explicitly shows the wavelength dependence, and is presented as dashed lines in the figure. The Gaussian assumption is well satisfied when the number of molecules N is reduced so far (cluster C2) that they arrange approximately like a string along the z -axis, since their x - histogram is then Gaussian. For C2, $\Delta x_{\text{C2}} = \Delta y_{\text{C2}} \simeq (1.7, 3.0, 4.1) \mu\text{m}$ at $T = (12, 33, 67) \text{ mK}$ increase approximately with the square root of the temperature, and thus more strongly in relative terms than for C1. This leads to a more pronounced variation of $L(0)$ with temperature than for C1, see Fig. 4 (d). The small values $\Delta x_{\text{C2}}, \Delta y_{\text{C2}}$ lead to a substantial $L(0) \simeq 0.3$ already for $\lambda \simeq 10 \mu\text{m}$ when $T = 13 \text{ mK}$.

For the C1 cluster the Gaussian assumption is not correct (see histogram in Fig. 4 (a)), therefore deviations between $L_g(0)$ and $L(0)$ are visible in Fig. 4 (d) for intermediate and small wavelengths. Heuristically, we find that the expression $L_{\text{sp}}(0) = J_0(2\pi\sqrt{2}\Delta x/\lambda)^2$, the result for a single ion harmonically oscillating along the x axis [37], provides a better description of the exact values because of the similarity in the probability distributions of the x coordinate values.

In summary, the simulations indicate that even for only moderately cold ensembles ($T \simeq 70 \text{ mK}$) and for a relatively small value $\lambda_{\text{rot,min}} = 228 \mu\text{m}$ ($f_{\text{rot,max}} = 1.3 \text{ THz}$) strong signatures of Lamb-Dicke confinement in rotational spectroscopy with transverse incidence can be expected. For string-like ion clusters a similar signature might be possible also for *axial* irradiation, but only at the lowest temperatures ($T \simeq 10 \text{ mK}$), when ion position changes are infrequent. This case will be the subject of future experimental studies.

B. Experimental Apparatus

The ion trap apparatus used in the present work, Fig. 5 is based on the device used previously [5, 38–40], and upgraded in several respects: (i) fully computer-controlled operation, (ii) accurate magnetic field control via solenoid pairs, (iii) improved frequency stabilization of the rotational cooling lasers L-RC1 and L-RC2, (iv) improved THz source frequency control.

The vacuum chamber housing the ion trap provides ultra-high vacuum conditions (3×10^{-11} mbar), minimizing spectral broadening and shifts due to ion - background gas collisions. Electron impact ionization inside the ion trap volume is used to generate Beryllium ions from Be atoms emitted by a hot filament and HD^+ ions from HD gas injected into the chamber. 313 nm radiation laser cools the Beryllium ions which sympathetically cool the HD^+ ions, resulting in a structured ion cluster as shown in Fig. 1. Subsequently, radiation fields at $5.48 \mu\text{m}$ and $2.71 \mu\text{m}$ perform rotational cooling. The 1.3 THz radiation for rotational spectroscopy propagates at 90 degrees with respect to the ion trap axis and thus the ion cluster axis, in order to provide the LDR. The beam radius at the center of the trap is approximately 1 mm. A CCD camera images the cluster's spatial structure, allowing for a direct observation of the spatial confinement and also comparison with molecular dynamics simulations. The photo-multiplier tube detects the fluorescence of the Be^+ ions, and also provides the signal for the spectroscopy.

The THz system consists of a hydrogen maser, whose frequency, $f_{\text{H}} \simeq 1.4$ GHz, is down-converted to 10 MHz and then used as reference for a microwave synthesizer operating at $f_{\text{mmw}/72} = 18.262$ GHz. Its output is converted in a $\times 72$ multiplier/amplifier chain to $f_{\text{rot}} = 1.31$ THz [41]. We verified the high spectral purity of the THz wave at the intermediate frequency 18.251 GHz, close to $f_{\text{mmw}/72}$. The setup used is shown in Fig. 6 (inset). The repetition rate $f_{\text{rep}} \simeq 250$ MHz of a fiber-based optical frequency comb is stabilized by phase-locking the beat frequency between an ultra-stable reference laser at $1.5 \mu\text{m}$ (L-ULE, with optical frequency f_{ULE} [42]) and a nearby comb mode (mode number $n \simeq 7.8 \times 10^5$) to a (maser-referenced) DDS set at $f_{\text{DDS}} = 50$ MHz, by controlling the repetition rate. The comb carrier-envelope offset frequency f_{CEO} is independently stabilized to the H-maser. The absolute frequency stability of the reference laser is therefore transferred to the repetition rate, $f_{\text{rep}} = (f_{\text{ULE}} - f_{\text{DDS}} - f_{\text{CEO}})/n$. Comb radiation at $1.5 \mu\text{m}$ is detected by a fast photo-

detector, and an RF signal arising from the 73rd harmonic of the repetition rate, $f_{\text{rep}\times 73}$, is generated. This harmonic is chosen since it can be set close to $f_{\text{mmw}/72}$. The difference frequency between $f_{\text{rep}\times 73}$ and $f_{\text{mmw}/72}$ is generated using a mixer and is analyzed using an FFT-based spectrum analyzer. Fig. 6 shows the line width of the difference frequency signal, which is 86 mHz. Based on this value and previous characterizations [41], we estimate a line width < 10 Hz at 1.3 THz. We can also infer the long-term frequency stability of the THz wave, by comparing the maser frequency to a GPS-derived 1 PPS signal and to a cryogenic silicon optical resonator [43]. The residual instability is negligible ($< 1 \times 10^{-13}$ for integration times $\tau > 10$ s) and so is drift.

C. Laser rotational cooling

In the present experiment, when molecular ions are generated and trapped and reach thermal equilibrium, the $(v = 0, N = 0)$ level's population is $\simeq 10\%$, and thus only $\simeq 1\%$ is in a single state $|g, J_z\rangle$. Therefore, before spectroscopy, we apply rotational laser cooling [39] (lasers L-RC1, L-RC2 in Fig. 5), to increase significantly the population in $(v = 0, N = 0)$, a procedure which also increases the population in the Zeeman states $|g, J_z\rangle$ to a level which can be observed.

We apply two laser fields which drive the fundamental vibrational transition $(v = 0, N = 2) \rightarrow (v' = 1, N' = 1)$, and the overtone vibrational transition $(v = 0, N = 1) \rightarrow (v' = 2, N' = 0)$. Because of quantum mechanical selection rules, repeated absorption - spontaneous emission cycles transfer the majority of the ion population into the ground state $(v = 0, N = 0)$.

A distributed feedback (DFB) laser at $2.71 \mu\text{m}$ is used to excite the overtone vibrational transition (L-RC1 in Fig. 5). The laser is frequency stabilized to a CO_2 gas transition using an offset locking technique [44] to bridge the frequency gap between the CO_2 transition and the HD^+ transition frequency. We use a quantum cascade laser (QCL) to drive the fundamental transition at $5.48 \mu\text{m}$ (L-RC2 in Fig. 5), whose frequency is stabilized to the side of a fringe of an NH_3 molecular transition.

D. Experimental sequence.

The preparation and spectroscopy sequence consists of the following steps: (1) HD⁺ generation by electron impact ionization; (2) impurity ion removal procedures; (3) rotational cooling for $t_{rc} = 35$ s; (4) secular excitation for $t_{se} = 3$ s, with rotational cooling lasers on; (5) during $t_{det} = 3$ s, the rotational cooling lasers are blocked, while THz radiation, and the 1.42 μ m and 266 nm waves for REMPD are on; (6) secular excitation during t_{se} . The signal is obtained from the difference in Be⁺ fluorescence recorded during intervals (4) and (6).

The magnetic field is set to 1.1 G along the trap axis z , except during step (5), where it is set to a smaller value B , sufficient to produce Zeeman splitting of most components of the studied transition. The sequence is repeated a number of times sufficient to obtain a reasonable signal-to-noise ratio. Be⁺ ions are reloaded every 100 to 150 sequences.

E. Rotational transition

The fundamental rotational transition of the molecular ion used here has an important spin structure because of the nonzero electron and nuclear magnetic moments [33]. While in the ground rovibrational level ($v = 0, N = 0$) they give rise to 4 spin states (having total angular momentum $J = 0, 1, 2$), in the first excited rotational level ($v = 0, N' = 1$) the number increases to 10 spin states (having $J' = 0, 1, 2, 3$), because of the additional presence of rotational angular momentum $N' \neq 0$. Fig. 2 shows the two spin states relevant to the spectroscopy of this work (for a complete diagram, see Fig. 2 in [40]). A controllable magnetic field lifts the total angular momentum projection (J_z) degeneracies, except for the two transitions T_±. We address transitions between two individual Zeeman components $|g, J_z\rangle$ of the $J = 2$ spin state of the $N = 0$ - level, and two components $|e, J'_z\rangle$ of the $J' = 3$ spin state of the $N' = 1$ - level. The transitions T₊: $J_z = 2 \rightarrow J'_z = 3$ and T₋: $J_z = -2 \rightarrow J'_z = -3$, shown by green arrows in Fig. 2, are transitions between stretched states (states of maximal total angular momentum J and maximal projection J_z) and have been previously identified as exhibiting particularly low Zeeman shifts [25, 45].

F. *Ab initio* theory of the HD⁺ rotational transition

The transition frequency $f_{\text{rot,theory}}$ involves two contributions. The first is the spin-averaged frequency $f_{\text{spin-avg}}$. We have computed it with very high precision using the same technique as in [31], obtaining

$$f_{\text{spin-avg}} = 1\,314\,925.752\,627(18) \text{ MHz},$$

with the relative uncertainty 1.4×10^{-11} . The second contribution is the hyperfine shift f_{spin} due to spin interactions (including coupling with the total orbital angular momentum), $f_{\text{spin}} = [E_{\text{spin}}(|u\rangle) - E_{\text{spin}}(|l\rangle)]/h$. Here $E_{\text{spin}}(|l\rangle)$ and $E_{\text{spin}}(|u\rangle)$ are the hyperfine spin energy shifts for the individual lower and upper states. So far, they have been calculated within the Breit-Pauli approximation only [33]. The spin energy shifts of the stretched states $|g, J_z = \pm 2\rangle$ and $|e, J'_z = \pm 3\rangle$ in a finite magnetic field can be readily computed using the algebraic expression (Eq. (6) in [25]),

$$\begin{aligned} & E_{\text{spin}}(v, N, J = L + 2, J_z = \pm J, B)/h = \\ & \pm(2E_{10}N + E_{11} + 2E_{12} + E_{13})B/2 + E_4/4 + E_5/2 \\ & + (E_1 + E_2 + 2E_3 + E_6 + 2E_7 + 2E_8 + E_9)N/2 \\ & - (2E_6 + 4E_7 + 4E_8 + 2E_9)N^2/2, \end{aligned}$$

where $E_i = E_i(v, N)$ are the coefficients of the effective spin Hamiltonian [25, 33]. Since the $J = 2 \rightarrow J' = 3$ transition keeps the spin function untouched, the hyperfine shift f_{spin} is most sensitive to the electron spin-orbit interaction $E_1(v = 0, N = 1)(\mathbf{s}_e \cdot \mathbf{N})$, where $E_1(v = 0, N = 1) \simeq 32 \text{ MHz}$ [33]. The spin-spin interactions, proportional to E_4 and E_5 , which are known with much higher precision than the other coefficients [30], give a much smaller contribution to f_{spin} , due to the similarity of the spin wave functions that leads to a substantial cancellation. The hyperfine shift is

$$f_{\text{spin}} = 10.0747(10) \text{ MHz}. \quad (4)$$

Summing both above contributions we obtain eq. (1).

In order to improve the 1-kHz theoretical uncertainty of f_{spin} it will be necessary to calculate the higher-order corrections to the coefficient E_1 . This particular sensitivity of the

observed transition on the accuracy of the effective spin Hamiltonian is characteristic for rotational transitions. For vibrational transitions, the much larger ratio of $f_{\text{spin-avg}}$ to f_{spin} reduces the sensitivity significantly. This is the case for the most intensive hyperfine components of the transitions (for which $|f_{\text{spin}}| < 100$ MHz), and the Breit-Pauli approximation is then in most cases sufficient to guarantee a fractional uncertainty of the total transition frequency comparable to the fractional uncertainty of the theoretical spin-averaged frequency.

It is important to note that the theoretical considerations of the spin-averaged and the hyperfine spin shift contributions to $f_{\text{rot,theory}}$ have recently been confirmed through a comparison, respectively, with one particular rovibrational transition frequency of HD^+ at the 1.1 ppb level [16] and with several spin transition frequencies (i.e. radio-frequency transitions) of H_2^+ at the ppm level [30].

G. Systematic shifts

We have previously computed most relevant sensitivities of the rotational transition to external perturbations: Zeeman shift [25], electric quadrupole shift [45], d.c. Stark shift, black-body radiation shift, and spin-state dependence of the d.c. Stark and light shift [46]. The quadratic Zeeman shift is zero for the transitions T_{\pm} .

For the experimental parameters of our trap, the cluster shape, and the moderate intensities of the radiation fields, the shifts are all small, except for the Zeeman shift. Since the orientation of the quantization axis and the populations of the lower Zeeman states are unknown, we assign an uncertainty equal to half the Zeeman splitting of T_+ and T_- , 0.22 kHz. The d.c. Stark shift has been computed taking into account ion trajectories and Coulomb fields, also allowing for d.c. offset potentials, and is less than 10 Hz. Collision shifts related to background gas are negligible due to the UHV conditions. One finite shift is the light shift induced by the 266 nm dissociation laser (35 mW power). In order to compute it, we have performed a precision calculation of the a.c. polarisabilities of the lower and upper rotational levels using the procedure described in [46]. We obtained the scalar (s) and tensor (t) polarisabilities $\alpha_s(v = 0, N = 0(1), \lambda = 266.0 \text{ nm}) = 3.677(3.687)$, $\alpha_t(v = 0, N = 0(1), \lambda = 266.0 \text{ nm}) = 0(-1.044)$, in atomic units. For the considered transitions, the shift is 7 (40) Hz. In total, we obtain a frequency correction of 0.0(3) kHz.

In future studies, any light shifts from the dissociation laser and from the 1.4 μm laser

could be avoided by applying these lasers only after the rotational excitation. If the Zeeman pair were split and resolved, the Zeeman shift uncertainty should be reduced at least 10-fold. This would then allow a total systematic uncertainty of $< 3 \times 10^{-11}$.

ACKNOWLEDGMENTS

This work has been partially funded by DFG project Schi 431/21-1. We thank U. Rosowski for important assistance with the frequency comb, A. Nevsky for assistance with a laser system, E. Wiens for characterizing H-maser instability, R. Gusek and P. Dutkiewicz for electronics development, J. Scheuer and M. Melzer for assistance, and S. Schlemmer (Universität zu Köln) for equipment loans. We thank K. Brown (Georgia Institute of Technology) for useful discussions and suggestions.

Corresponding author, step.schiller@hhu.de

Contributions

S.A. and M.G.H. developed the apparatus and performed the experiments, S.A., M.G.H., and S.S. analyzed the data, S.A., S.S. and V.I.K. performed theoretical calculations, S.S. conceived the study, supervised the work and wrote the paper.

Competing financial interests.

The authors declare no competing financial interests.

-
- [1] M. Raizen, J. Gilligan, J. Bergquist, W. Itano, D. Wineland, Ionic crystals in a linear Paul trap, *Phys. Rev. A* 45 (1992) 6493. doi:10.1103/PhysRevA.45.6493.
 - [2] I. Waki, S. Kassner, G. Birkel, H. Walther, Observation of ordered structures of laser-cooled ions in a quadrupole storage ring, *Phys. Rev. Lett.* 68 (1992) 2007. doi:10.1103/PhysRevLett.68.2007.
 - [3] P. Rowe, L. Hornekaer, C. Brodersen, M. Drewsen, S. Hangst, J. Schiffer, Sympathetic Crystallization of Trapped Ions, *Phys. Rev. Lett.* 82 (1999) 2071. doi:10.1103/PhysRevLett.82.2071.
 - [4] M. D. Barrett, B. DeMarco, T. Schaetz, V. Meyer, D. Leibfried, J. Britton, J. Chiaverini, W. M. Itano, B. Jelenković, J. D. Jost, C. Langer, T. Rosenband, D. J. Wineland, Sympathetic

- cooling of ${}^9\text{Be}^+$ and ${}^{24}\text{Mg}^+$ for quantum logic, *Phys. Rev. A* 68 (2003) 042302. doi:10.1103/PhysRevA.68.042302.
- [5] U. Bressel, A. Borodin, J. Shen, M. Hansen, I. Ernsting, S. Schiller, Manipulation of individual hyperfine states in cold trapped molecular ions and application to HD^+ frequency metrology, *Phys. Rev. Lett.* 108 (2012) 183003. doi:10.1103/PhysRevLett.108.183003.
- [6] D. J. Berkeland, J. D. Miller, J. C. Bergquist, W. M. Itano, D. J. Wineland, Laser-cooled mercury ion frequency standard, *Phys. Rev. Lett.* 80 (1998) 2089. doi:10.1103/PhysRevLett.80.2089.
- [7] C. Townes, A. Schawlow, *Microwave Spectroscopy*, Dover Publications, Inc., New York, 1975.
- [8] P. Jusko, O. Asvany, A.-C. Wallerstein, S. Brünken, S. Schlemmer, Two-Photon Rotational Action Spectroscopy of Cold OH^- at 1 ppb Accuracy, *Phys. Rev. Lett.* 112 (2014) 253005. doi:10.1103/PhysRevLett.112.253005.
- [9] S. Schiller, V. Korobov, Test of time-dependence of the electron and nuclear masses with ultracold molecules, *Phys. Rev. A* 71 (2005) 032505. doi:10.1103/PhysRevA.71.032505.
- [10] A. Shelkovich, R. J. Butcher, C. Chardonnet, A. Amy-Klein, Stability of the Proton-to-Electron Mass Ratio, *Phys. Rev. Lett.* 100 (2008) 150810. doi:10.1103/PhysRevLett.100.150801.
- [11] J.-P. Uzan, Varying constants, gravitation and cosmology, *Living Rev. Relativity* 14 (2011) 2. URL <http://www.livingreviews.org/lrr-2011-2>
- [12] R. M. Godun, P. B. R. Nisbet-Jones, J. M. Jones, S. A. King, L. A. M. Johnson, H. S. Margolis, K. Szymaniec, S. N. Lea, K. Bongs, P. Gill, Frequency Ratio of Two Optical Clock Transitions in ${}^{171}\text{Yb}^+$ and Constraints on the Time Variation of Fundamental Constants, *Phys. Rev. Lett.* 113 (2014) 210801. doi:10.1103/PhysRevLett.113.210801.
- [13] N. Huntemann, B. Lipphardt, C. Tamm, V. Gerginov, S. Weyers, E. Peik, Improved Limit on a Temporal Variation of m_p/m_e from Comparisons of Yb^+ and Cs Atomic Clocks, *Phys. Rev. Lett.* 113 (2014) 210802. doi:10.1103/PhysRevLett.113.210802.
- [14] B. Roth, J. Koelemeij, S. Schiller, L. Hilico, J.-P. Karr, V. Korobov, D. Bakalov, Precision Physics of Simple Atomic Systems, Vol. 745 of *Lect. Notes Phys.*, Springer, 2008, Ch. Precision Spectroscopy of Molecular Hydrogen Ions: Towards Frequency Metrology of Particle Masses, pp. 205 – 232. doi:10.1007/978-3-540-75479-4_12.
- [15] J. C. J. Koelemeij, B. Roth, A. Wicht, I. Ernsting, S. Schiller, Vibrational spectroscopy of

- HD⁺ with 2-ppb accuracy, *Phys. Rev. Lett.* 98 (2007) 173002. doi:10.1103/PhysRevLett.98.173002.
- [16] J. Biesheuvel, J.-P. Karr, L. Hilico, K. S. E. Eikema, W. Ubachs, J. C. J. Koelemeij, Probing QED and fundamental constants through laser spectroscopy of vibrational transitions in HD⁺, *Nature Comm.* 7 (2016) 10385. doi:10.1038/ncomms10385.
- [17] R. S. Winton, W. Gordy, High-precision millimeter-wave spectroscopy with Lamb dip, *Phys. Lett. A* 32 (1970) 219 – 220. doi:10.1016/0375-9601(70)90287-2.
- [18] G. Cazzoli, L. Dore, Observation of crossing resonances in the hyperfine structure of the $J = 1 \leftarrow 0$ transition of DC¹⁵N, *J. Molecular Spectroscopy* 143 (1990) 231 – 236. doi:10.1016/0022-2852(91)90087-Q.
- [19] G. Winnewisser, S. P. Belov, T. Klaus, R. Schieder, Sub-doppler measurements on the rotational transitions of carbon monoxide, *J. Molecular Spectroscopy* 184 (1997) 468–472. doi:10.1006/jmsp.1997.7341.
- [20] G. Cazzoli, C. Puzzarini, Sub-Doppler Resolution in the THz Frequency Domain: 1 kHz Accuracy at 1 THz by Exploiting the Lamb-Dip Technique, *J. Phys. Chem. A* 117 (2013) 13759 – 13766. doi:10.1021/jp407980f.
- [21] R. H. Dicke, The effect of collisions upon the Doppler width of spectral lines, *Phys. Rev.* 89 (1953) 472–473. doi:10.1103/PhysRev.89.472.
- [22] M. Germann, X. Tong, S. Willitsch, Observation of dipole-forbidden transitions in sympathetically cooled, state-selected, homonuclear diatomic molecular ions, *Nature Physics* 10 (2014) 820–824. doi:10.1038/nphys3085.
- [23] F. Wolf, Y. Wan, J. Heip, F. Gebert, C. Shi, P. Schmidt, Non-destructive state detection for quantum logic spectroscopy of molecular ions, *Nature* 530 (2016) 457–460. doi:10.1038/nature16513.
- [24] C. Chou, C. Kurz, D. Hume, P. Plessow, D. R. Leibbrandt, D. Leibfried, Preparation and coherent manipulation of pure quantum states of a single molecular ion, *Nature* 545 (2017) 203–207. doi:10.1038/nature22338.
- [25] D. Bakalov, V. Korobov, S. Schiller, Magnetic field effects in the transitions of the HD⁺ molecular ion and precision spectroscopy, *J. Phys. B: At. Mol. Opt. Phys.* 44 (2011) 025003, corrigendum: *J. Phys. B: At. Mol. Opt. Phys.* 45, 049501 (2012).
- [26] J. Shen, A. Borodin, S. Schiller, A simple method for characterization of the magnetic

- field in an ion trap using Be^+ ions, Eur. Phys. J. D 68 (2014) 359. doi:10.1140/epjd/e2014-50360-7.
- [27] P. J. Mohr, D. B. Newell, B. N. Taylor, CODATA recommended values of the fundamental physical constants: 2014, Rev. Mod. Phys. 88 (2016) 035009. doi:10.1103/RevModPhys.88.035009.
- [28] V. I. Korobov, L. Hilico, J. P. Karr, Theoretical transition frequencies beyond 0.1 ppb accuracy in H_2^+ , HD^+ , and antiprotonic helium, Phys. Rev. A 89 (2014) 032511. doi:10.1103/PhysRevA.89.032511.
- [29] V. I. Korobov, L. Hilico, J.-P. Karr, $m\alpha^7$ -Order Corrections in the Hydrogen Molecular Ions and Antiprotonic Helium, Phys. Rev. Lett. 112 (2014) 103003. doi:10.1103/PhysRevLett.112.103003.
- [30] V. I. Korobov, J. C. J. Koelemeij, L. Hilico, J.-P. Karr, Theoretical Hyperfine Structure of the Molecular Hydrogen Ion at the 1 ppm Level, Phys. Rev. Lett. 116 (2016) 053003. doi:10.1103/PhysRevLett.116.053003.
- [31] V. I. Korobov, L. Hilico, J.-P. Karr, Fundamental Transitions and Ionization Energies of the Hydrogen Molecular Ions with Few ppt Uncertainty, Phys. Rev. Lett. 118 (2017) 233001. doi:10.1103/PhysRevLett.118.233001.
- [32] F. Constantin, Feasibility of two-photon rotational spectroscopy on trapped HD^+ , in: Proc. SPIE 9900, Quantum Optics, Vol. 99001B, 2016. doi:10.1117/12.2227817.
- [33] D. Bakalov, V. I. Korobov, S. Schiller, High-precision calculation of the hyperfine structure of the HD^+ ion, Phys. Rev. Lett. 97 (2006) 243001. doi:10.1103/PhysRevLett.97.243001.
- [34] L. Hornekær, N. Kjærgaard, A. M. Thommesen, M. Drewsen, Structural Properties of Two-Component Coulomb Crystals in Linear Paul Traps, Phys. Rev. Lett. 86 (2001) 1994. doi:10.1103/PhysRevLett.86.1994.
- [35] C. B. Zhang, D. Offenbergh, B. Roth, M. A. Wilson, S. Schiller, Molecular-dynamics simulations of cold single-species and multispecies ion ensembles in a linear Paul trap, Phys. Rev. A 76 (2007) 012719. doi:10.1103/PhysRevA.76.012719.
- [36] H. Cramér, Random Variables and Probability Distributions, Cambridge Tracts on Mathematics and Mathematical Physics, No. 36, Cambridge University Press, Cambridge, UK, 1970.
- [37] D. J. Berkeland, J. D. Miller, J. C. Bergquist, W. M. Itano, D. J. Wineland, Minimization

- of ion micromotion in Paul trap, *J. Appl. Phys.* 83 (10) (1998) 5025–5033. doi:10.1063/1.367318.
- [38] P. Blythe, B. Roth, U. Fröhlich, H. Wenz, S. Schiller, Production of ultracold trapped molecular hydrogen ions, *Phys. Rev. Lett.* 95 (2005) 183002. doi:10.1103/PhysRevLett.95.183002.
- [39] T. Schneider, B. Roth, H. Duncker, I. Ernsting, S. Schiller, All-optical preparation of molecular ions in the rovibrational ground state, *Nature Physics* 6 (2010) 275 – 278. doi:10.1038/NPHYS1605.
- [40] J. Shen, A. Borodin, M. Hansen, S. Schiller, Observation of a rotational transition of trapped and sympathetically cooled molecular ions, *Phys. Rev. A* 85 (2012) 032519. doi:10.1103/PhysRevA.85.032519.
- [41] S. Schiller, B. Roth, F. Lewen, O. Ricken, M. Wiedner, Ultra-narrow-linewidth continuous-wave THz sources based on multiplier chains, *Appl. Phys. B* 95 (2009) 55–61. doi:10.1007/s00340-008-3279-9.
- [42] E. Wiens, A. Y. Nevsky, S. Schiller, Resonator with ultrahigh length stability as a probe for equivalence-principle-violating physics, *Phys. Rev. Lett.* 117 (2016) 271102. doi:10.1103/PhysRevLett.117.271102.
- [43] E. Wiens, Q. Chen, I. Ernsting, H. Luckmann, A. Y. Nevsky, U. Rosowski, S. Schiller, A silicon single-crystal cryogenic optical resonator, *Opt. Lett.* 39 (2014) 3242. doi:10.1103/PhysRevLett.117.271102.
- [44] A. Y. Nevsky, S. Alighanbari, Q. Chen, I. Ernsting, S. Vasilyev, S. Schiller, G. Barwood, P. Gill, N. Poli, G. M. Tino, Robust frequency stabilization of multiple spectroscopy lasers with large and tunable offset frequencies, *Opt. Lett.* 38 (2013) 4903–6. doi:10.1364/OL.38.004903.
- [45] D. Bakalov, S. Schiller, The electric quadrupole moment of molecular hydrogen ions and their potential for a molecular ion clock, *Appl. Phys. B* 114 (2014) 213–230. doi:10.1007/s00340-013-5703-z.
- [46] S. Schiller, D. Bakalov, A. K. Bekbaev, V. I. Korobov, Static and dynamic polarizability and the Stark and blackbody-radiation frequency shifts of the molecular hydrogen ions H_2^+ , HD^+ , and D_2^+ , *Phys. Rev. A* 89 (2014) 052521. doi:10.1103/PhysRevA.89.052521.

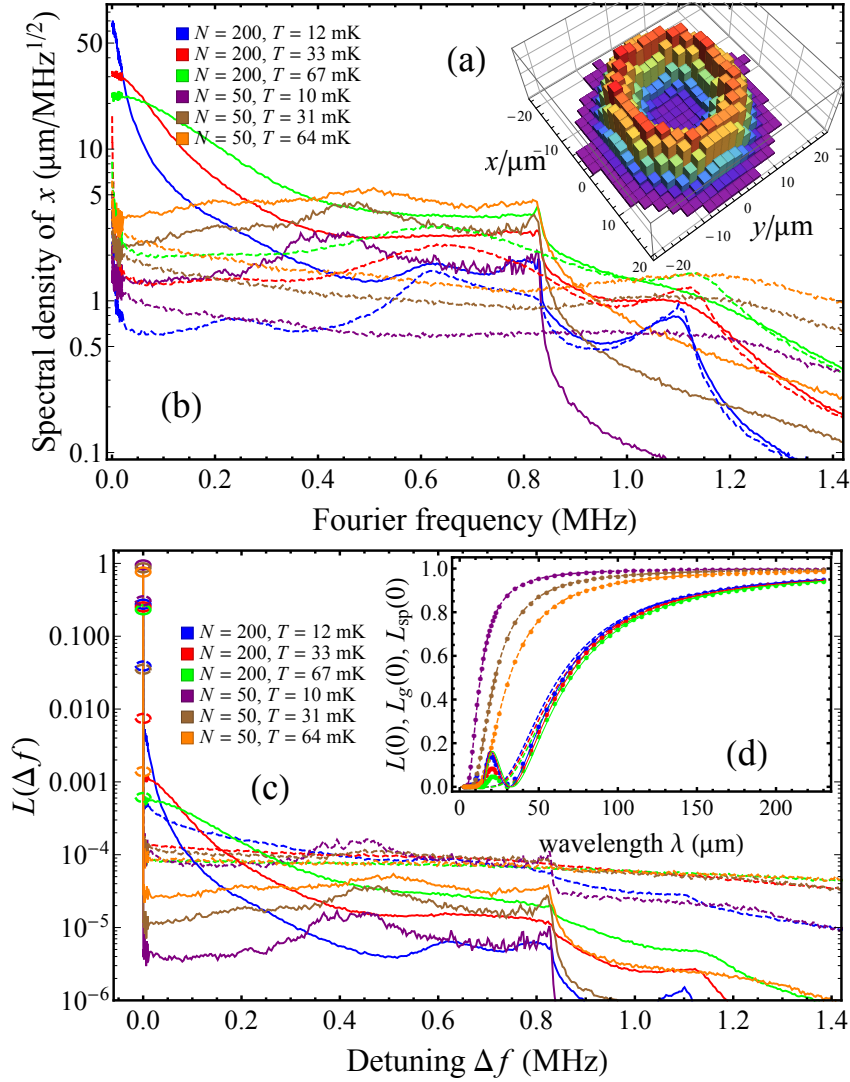


FIG. 4. Characteristics and consequences of the motion of molecular ions in laser-cooled Be^+/HD^+ Coulomb clusters at different temperatures. Cluster C1 (C2): $N = 200$ (50), $N_{\text{Be}^+} = 2000$ (500). Blue lines correspond to the situation in the experiment. (a) Compound histogram of the transverse positions (x_i, y_i) of five randomly chosen molecular ions in Cluster 1, at $T \approx 33$ mK; the ring shape is related to the fact that for the chosen ion numbers the molecular ions arrange and move in a tubular cylindrical structure. (b) Ensemble average of the linear spectral density of the x coordinate of the ions (full lines) and of the distance from the trap axis, $\rho = (x^2 + y^2)^{1/2}$ (dashed lines). The two spectra reflect the fact (evidenced by inspecting the ions' trajectories) that the transverse ion motion is a combination of a fast and small-range random motion perpendicular to the “tube” axis, described by $\rho_i(t)$, and of a slower azimuthal motion around the tube, having a wider range. (c) Qualitative spectral line shape $L(\Delta f)$, for two different wavelengths $\lambda = 50 \mu\text{m}$ (full), $10 \mu\text{m}$ (dashed). Only the positive detunings are shown. (d) Strength of the Lamb-Dicke peak ($\Delta f = 0$). Points: exact values $L(0)$; dashed and full lines: approximate expressions $L_g(0)$, $L_{sp}(0)$, respectively, defined in the text. Same colours in (b) and (c) and (d) correspond to the same cluster type and temperature. Transverse secular frequency of the molecular ions is 0.81 MHz; a corresponding feature is seen in the spectra of x and in the line shapes L .

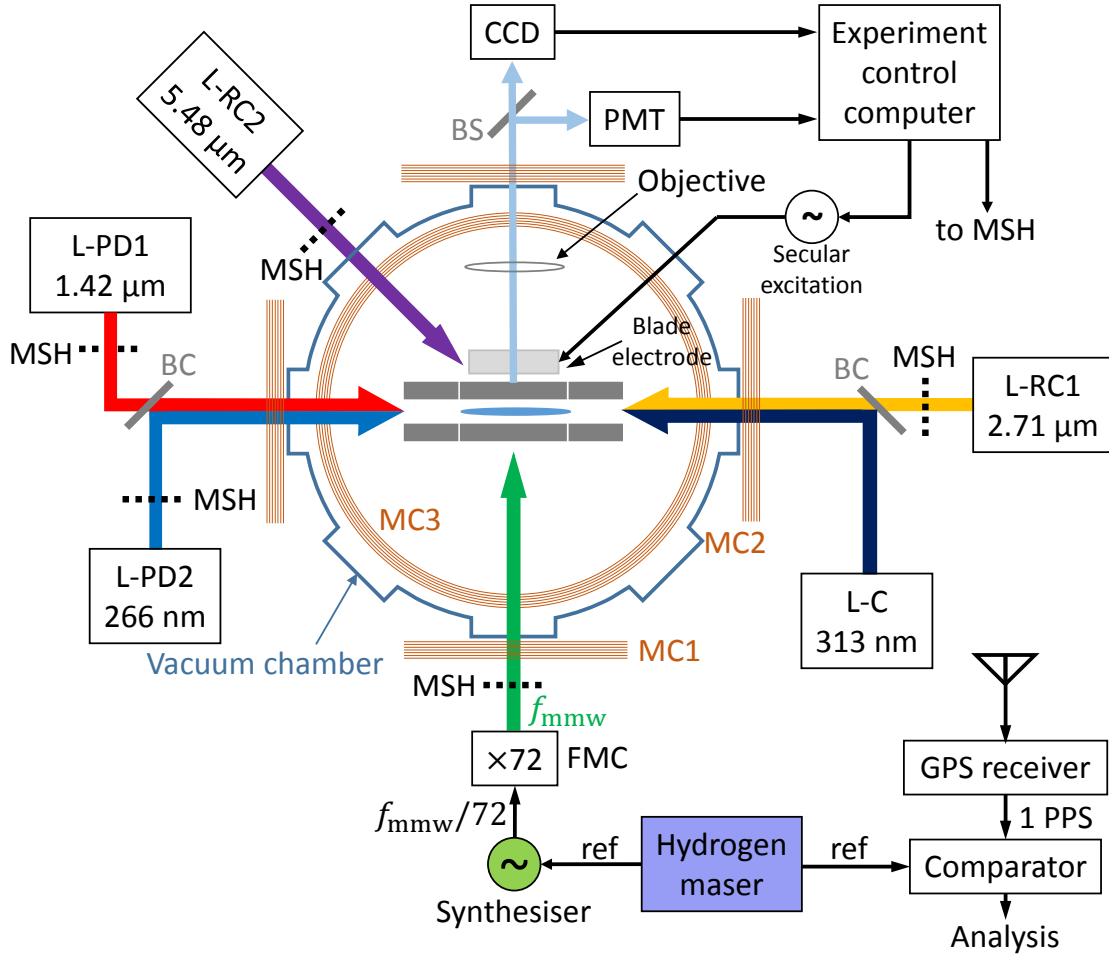


FIG. 5. Simplified schematic of the apparatus. The THz radiation (green arrow) propagates along x , perpendicularly to the ion cluster's axis. BC: beam combiner, BS: beam splitter, FMC: frequency multiplier chain, MSH: mechanical shutter, L-PD: photo-dissociation lasers, L-RC: rotational cooling lasers, L-C: Be^+ cooling laser, PMT: photo-multiplier tube, MC: magnetic coils, CCD: CCD camera. Beryllium oven, electron gun, and HD gas handling system are not shown.

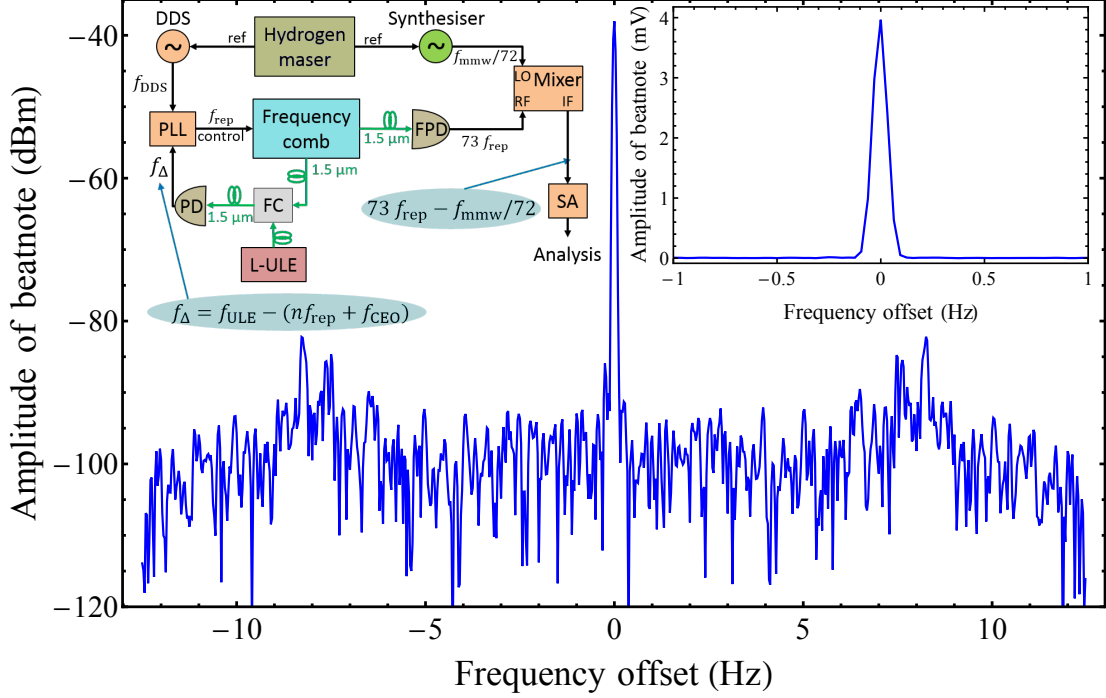


FIG. 6. THz line width characterization. Main plot: power spectrum of the signal oscillating at the difference between an intermediate frequency close to $f_{\text{mmw}}/72$ (synthesizer) and $f_{\text{rep}} \times 73$, the 73rd harmonic of the frequency comb's repetition rate. Full-width half-maximum is 86 mHz, with the resolution bandwidth being 31.25 mHz. Right inset: same as the main plot but the amplitude is in mV. Left inset: Schematic of the line-width measurement setup. FC: Fiber combiner, L-ULE: continuous-wave 1.5 μm semiconductor laser stabilized to an ultra-low expansion (ULE) glass cavity, PD: photo-detector, FPD: high-bandwidth photo-detector, SA: spectrum analyzer, PLL: phase lock feedback loop, DDS: direct digital synthesizer.